Journal of Solar Energy Research (JSER)

Journal homepage: www.jser.ut.ac.ir

A High Efficiency On-board Charger for Solar Powered Electric Vehicles Using a Novel Dual-output DC-DC Converter

P. Bayat[a], A. Baghramian[a,*]

[a] Department of Electrical Engineering, University of Guilan, Rasht, Iran; *Email: Alfred@guilan.ac.ir

ARTICLE INFO

Received: 11 Jun 2019
Received in revised form: 12 Jul 2019
Accepted: 31 Jul 2019
Available online: 01 Aug 2019

Keywords:
Battery charger;
DC-DC converter;
Photovoltaic (PV);
Solar powered electric vehicle (SPEV);

A B S T R A C T

Solar powered electric vehicles (SPEVs) charge their energy storages from photovoltaic (PV) panels via on-board charger. The battery charger for these vehicles is mainly dependent on the DC-DC stage. Accordingly, this paper proposes an on-board battery charger utilizing a novel dual-output isolated DC-DC converter to charge battery and supercapacitor (SC) simultaneously. This topology uses impedance quasi-Z source network and also integrates both switched-capacitors and coupled-inductor techniques to achieve higher voltage gain ratio. Furthermore, compared to the traditional battery chargers, due to the use of only two switches, the number of components, the system size and the corresponding cost can be reduced. The results obtained by computer simulation demonstrate that the high voltage gain is obtained for both battery and SC ports at lower values of duty ratio with an efficiency of more than 94.5%. Finally, experiments with a 150W prototype are demonstrated in the laboratory to investigate the performance and effectiveness of the proposed SPEVs charger.

1. Introduction

Growing environmental concerns coupled to the decreasing of fossil fuel energy sources stimulate highly research on new vehicle technologies. Solar powered electric vehicles (SPEVs) and hybrid electric vehicles (HEVs) appear to be one of the most promising technologies for reducing fuel consumption and pollutant emissions [1,2]. In SPEVs, the solar energy absorbed from the sun by the solar panels is converted into chemical energy, and stored in rechargeable batteries [3]. Also, these kinds of vehicles require a larger battery with much higher capacity [4, 5].

Without a doubt, the main obstacle in SPEVs advancement is the supply of efficient, stable and enough electrical energy for the electric motor [4].

In this context, many researchers have worked on ways to improve the efficiency of energy storage systems, which are generally divided into two categories. The first way is to focus on battery system itself [6-11], whereas the second solution is developing a suitable charging structure [12-15].

Many design methodologies have been proposed for battery systems in the past decades. The size, cost, battery market, battery economics, power management strategy and mechanical packaging are well discussed from different aspects in [6-9]. Lithium-ion, Lead Acid and Nickel Metal Hydride batteries are to mention a few types of batteries being used as energy storage systems to drive SPEVs. In [6], all the basic terms and information have been described in the context of battery systems. Also, design consideration of Nickel Metal Hydride battery along with its discharge and charge characteristics and cost performances of batteries over years have been described. Reference [7], has emphasized various aspects relating to the economics of Lead Acid batteries and the market dynamics which affect the battery industry. Furthermore, an overview of the utilization of different batteries and their use as energy storage systems as well as in SPEVs and HEVs is presented in [8], whreras the Lithium-ion battery will particularly be the center of discussion in this article.

In [10], the improved battery design of an electric vehicle is proposed to smoothly enhance the performance in many aspects; e.g. it has an extended lifespan and causes a lower maintenance and replacement cost, furthermore the speeding performance can be better with the help of this new battery design. Also, in [11], improved battery design and electrification of a HEV are investigated to improve the driving range as well as acceleration, maximum speed and reducing the consumption of current and power; in this design, the precise calculations have been considered using charge and discharge rates and chemical reactions.

From another point of view, an on-board charger is treated as the key technology for SPEVs, which can reduce end user range anxiety by allowing for the vehicle's battery to be charged from photovoltaic (PV) panels. While having such a system on-board the vehicle provides convenience, it also adds volume and weight. These types of chargers, typically includes a DC-DC converter, which it is responsible for changing the voltage level of the PV panels to the required voltage for battery charging [13, 14]. The efficiency of an on-board battery charger is mainly dependent on the DC-DC stage since the output voltage and current are regulated in this stage.

In recent years, various types of DC-DC converters are widely applied to on-board battery chargers. In general, these converters are divided into two categories: non-isolated and isolated [15, 16]. Although non-isolated charging that complies with all safety regulations is possible, a preferable structure of battery chargers is isolated. Also, for achieving higher reliability, the battery charging system needs galvanic isolation between the grid and vehicle. At the same time, it needs long life cycle, and small and light design is essential to apply on-board [17].

Single-ended primary-inductor converter is in the category of non-isolated topologies and it has been adopted for many applications such as battery chargers [18, 19] and power factor correction [20, 21]. This kind of converter can has a low input current ripple. However, it has several drawbacks. Low efficiency due to hard switching operation of the power switches and high voltage stresses of power semiconductor devices are the two major drawbacks of this converter [18-21]. When the voltage rating is higher, e.g. in high voltage applications, the $R_{ds}(on)$ of power switches (e.g., metal-oxide-semiconductor field-effect transistor (MOSFET)) is higher. So, it causes higher conduction loss at the same level current. Therefore, if the voltage stress is reduced at the same level current, the overall efficiency can be improved.

Aiming to provide higher voltage conversion ratios, many techniques for the non-isolated DC-DC converters e.g. switched-capacitors and coupled-inductor are presented. In switched-capacitors based converters, the input voltage is used to provide energy and the switched-capacitors are linked in series and supply energy to the load. Thus, the source voltage can be multiplied [22, 23]. The major problem of the switched-capacitor cells is voltage stress of the switches. Also high voltage rated devices make high conduction losses. Converters with couple inductor can provide high step-up voltage gain with low duty cycle and with a simple topology. However, the main problem of these converters is the high voltage stress of the switches due to leakage inductance [24-27].

A novel concept of an integrated non-isolated on-board battery charger is proposed in [28]. This structure integrates a non-isolated DC-DC converter and a high power DC-DC converter by sharing the semiconductor devices and mechanical elements. This proposed system has the advantages of higher power density and lower cost. However, when these two structures operate at the same time, the proposed structure cannot charge the low voltage battery, or an additional converter is required to regulate the output voltage. Moreover, the final efficiency of the system is low because of the multi-stage structure.

Another design of a non-isolated on-board charger for HEVs is presented in [29]. This topology consists of a series connected single-phase rectifier, buck converter, and boost converter for reducing current ripple of the input and the output by dividing the input current. However, such configurations (series or parallel structures) are costly, bulky and relatively complex in design and reduce overall efficiency as well as reliability of the system.

Most of isolated DC-DC converters include magnetic components, such as transformers. In recent years, various isolated DC-DC converters based on half-bridge and full-bridge topologies have been proposed [30-33]. The magnetic components, however, occupy a large volume and weight in the converter, and also produce non-negligible losses [31]. On the other hand, isolated topologies usually use a large number of switches, which decrease the reliability of the system and leading to increased losses and costs [32,33].

In [34], a new isolated converter with reduced conduction loss for battery on-board chargers in HEVs is proposed. This topology consists of a full-bridge converter integrated with a symmetric half-bridge converter in parallel; it has a lower secondary voltage stress, which can result in a reduction of secondary conduction loss. However, this converter has large reactive current flows due to the use of traditional full and half-bridge converters, which provides electrical stress on its switching elements and increase of power losses.

In order to improve the performance of DC-DC converter in on-board battery charger applications, a novel dc-dc converter is proposed in [35]. This converter achieves low voltage stress in the rectifying diodes. In spite of this topology needs a lot of components e.g. power switches and capacitors, which cause the increase in power loss, size, and weight. In addition, in order to maintain high efficiency under low power conditions, it is necessary to minimize the amount of semiconductor devices in the DC-DC converter. In order to overcome these defects, cascade topology is mainly considered [36]. In these structures two different converters are connected in series condition to boost the voltage level. In [36], a novel approach for on-board charger design without high-voltage electrolytic capacitors is proposed. It has the cascade structure of an isolated resonant converter with constant frequency and a discontinuous conduction mode boost converter with a harmonic modulation technique. In this topology, its operation is based on the one traditional boost converter so that it is not suitable for high output current applications.

As a conclusion, in term of the number of elements, isolated converters need much more components than non-isolated converters. In addition, the transformer and additional elements are directly connected with increasing the cost and space of the topology [32]. In the other hand, the non-isolated topologies have some problems, which are reversal of the ground between the input and the output, and additional passive components, to attach on the battery charger [15, 33]. Also, these type of converters have problems with the high-voltage stress of the components, because switches and diodes should tolerate the summation of the output and input voltages during operation. In order to stand high-voltage stress, the semiconductor devices should have high ratings. This gives rise to large conducting losses, because the drift region of the internal junction structure becomes longer.

In SPEVs, adding electric equipment like supercapacitors (SCs) along with battery might be the most important point in increasing competency of these vehicles. Hence, a combination of battery and SC may mitigate the rate capacity effect of high pulsed discharge current. Also SC can assist the battery pack in peak power demands which not only prolongs the battery life time, but also improves the vehicle acceleration [15].

By adding the SCs to the energy storage system, the charger must be capable of charging two separate power supplies. Also, as mentioned earlier, the battery charger for SPEVs is mainly dependent on the DC-DC stage. Accordingly, this paper focuses on the DC-DC converter for charging two separate power supplies. For this purpose, this study presents an on-board SPEVs battery charger utilizing a novel dual-output isolated DC-DC converter to charge battery and SC simultaneously. This topology uses impedance quasi-Z source network and also integrates both switched-capacitors and coupled-inductor techniques to achieve higher voltage gain ratio. Furthermore, compared to the traditional battery chargers, due to the use of only two switches, the number of components, the system size and the corresponding cost can be reduced.

In a nutshell, compared to aforementioned converters used for on-board battery chargers, the main novelties of this paper are:

- The proposed DC-DC converter can charge two outputs with different voltage levels simultaneously, e.g. battery pack along with SC module;

- This topology uses impedance quasi-Z source network and also integrates both switched-capacitors and coupled-inductor techniques to achieve higher voltage gain ratio;
- While the proposed topology has all the benefit mentioned in the before on-board battery charger, it has fewer components and higher efficiency;
- The proposed topology is compact due to the reduced components; consequently it is cost effective;
- The isolation has been done through coupled inductor with reduced turn's ratio;
- Only two power switches are used to achieve power flow control.

The paper is organized as follows. Section 2 presents the circuit configuration of the proposed dual-output converter. The analyses of the operational modes is given in section 3. Section 4 shows the steady-state analysis. Comparison and performance assessment is presented in sections 5. Section 6 provides simulation and experimental results. Finally, section 7 is devoted to give a conclusion.

2. Circuit Configuration of the Proposed Dual-output DC-DC Converter

The proposed dual-output DC-DC converter circuit is shown in Fig. 1. The low DC input voltage (output voltage of the PV panels) is V_{PV} and only two switches are used along with six diodes (D_{in}, D_{SC}, D_1, D_2, D_3 and D_o), an input inductor (L_1), a coupled-inductor and five capacitors (C_1, C_2, C_3, C_4 and C_o). In order to perform the steady state analysis, several assumptions are made as follows:

- The converter operates in continues conduction mode (CCM) condition.
- The semiconductor components (switches and diodes) are ideal.
- All capacitors are large enough. Thus, their voltages are considered as constant values.
- Input inductor is large enough, so the input current ripple can be ignored.
- The coupled-inductor is modeled as an ideal transformer with turns ratio $N=N_S/N_P$, magnetizing inductor L_m and leakage inductors L_{K1} and L_{K2}.
- Coupling coefficient of the coupled-inductor is expressed by $\beta=L_m/(L_m+L_{K1})$.

3. Principles of Operation and Analysis

Fig. 2 and Fig. 3 show the typical waveforms of voltages and currents of the proposed topology and the topological stages for one switching cycle, respectively. There are six topological stages within each switching cycle. The time durations I, II and IV are neglected, because they are very short and have no significant effect on DC analysis and modeling process. Consequently, the main operation modes are III, V and VI, which shown in Fig. 2.

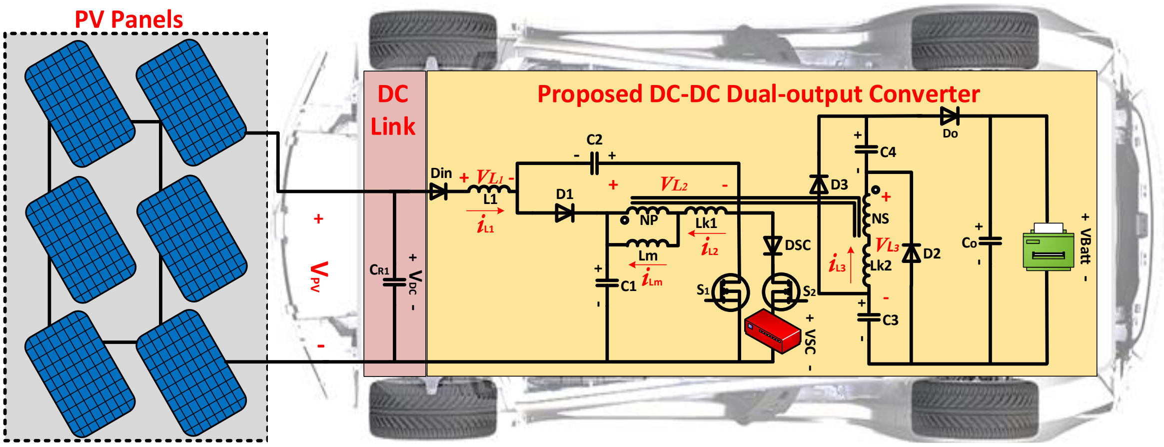

Figure 1. Detailed representation of the proposed dual-output DC-DC converter

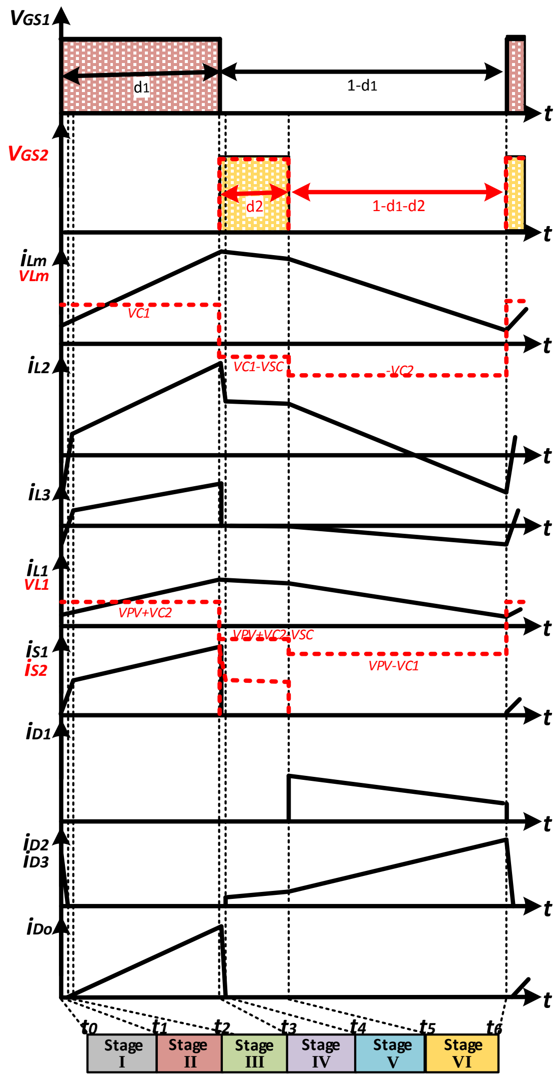

Figure 2. Typical waveforms of voltages and currents of the proposed dual-output DC-DC converter

Stage I ([t_0, t_1]) [see Fig. 3(a)]: In this time interval, at t=t_0, the power switch S_1 is turned ON while switch S_2 is OFF. The diodes D_1, D_{SC} and D_o are reversed bias and the diodes D_{in}, D_2 and D_3 are forward-biased. The DC link voltage (V_{PV}), transfers energy to the magnetizing inductor (L_m) and leakage inductor (L_{k1}). The capacitors C_3 and C_4 receive energy form the leakage inductor (L_{k2}) in parallel. The output capacitor C_o supplies the load at this state. The capacitor C_2 is discharged.

Stage II ([t_1, t_2]) [see Fig. 3(b)]: At the beginning of this time interval, D_{in} and D_o are forward-biased; furthermore, D_1, D_2, D_3 and D_{SC} are reverse-biased. Switches S_1 and S_2 remain ON and OFF, respectively. The capacitor C_2 discharged and the leakage inductor (L_{k1}) receives energy the same as stage I. The capacitors C_3 and C_4 are transfer their energy to the battery port.

Stage III ([t_2, t_3]) [see Fig. 3(b)]: In this stage, the input inductor (L_1) and the primary side of the coupled-inductor are receive energy from the DC link voltage (V_{PV}). The current of input inductor increases linearly. The other circuit conditions are the same as in the last time interval. The energy of magnetizing inductance (L_m) is delivered to the secondary winding of the coupled-inductor, where it is linked in series with the capacitors C_3 and C_4, to charge them to a voltage level depending on the conversion ratio and also to release energy to output capacitor C_o and battery port. In this stage by considering that $V_{C3}=V_{C4}=N\beta V_{C2}$, the following equations can be written in this state of operation:

$$V_{L1}^{III}=V_{PV}+V_{C_2} \tag{1}$$

$$V_{L2}^{III}=V_{C_1} \tag{2}$$

$$V_{L3}^{III}=N\beta\, V_{C_1} \tag{3}$$

$$V_{Batt}=V_{L3}^{III}+V_{C_3}+V_{C_4}=N\beta(2V_{C_2}+V_{C_1}) \tag{4}$$

Stage IV ([t_3, t_4]) [see Fig. 3(c)]: At the beginning of this mode, S_1 and S_2 are turned OFF and turned ON, respectively. The diodes D_{in}, D_{SC} and D_o are conducting, whereas the diodes D_1, D_2 and D_3 are reverse-biased. The SC port receives energy from both DC link voltage (V_{PV}) and input inductor (L_1). Also leakage inductor (L_{k2}), discharges its energy to the capacitors C_3 and C_4 and to the battery port.

Stage V ([t_4, t_5]) [see Fig. 3(d)]: At t=t_4, diodes D_2 and D_3 are forward-biased, whereas, diode D_o is reverse-biased. Switches S_1 and S_2 and the diodes D_1 and D_{SC} keep their states as in time interval IV. Also similar to the previous stage, the SC port receives energy from both DC link voltage (V_{PV}) and input inductor (L_1) and leakage inductor (L_{k2}), discharges its energy to the capacitors C_3 and C_4 and to the battery port. Output capacitor C_o release energy to output load (battery). Following equations can be written for this state of operation:

$$V_{L1}^{V}=V_{PV}+V_{C_2}-V_{SC} \tag{5}$$

$$V_{L2}^{V}=V_{C_1}-V_{SC} \tag{6}$$

$$V_{L3}^{V}=N\beta(V_{C_1}-V_{SC}) \tag{7}$$

Stage VI ([t_5, t_6]) [see Fig. 3(e)]: During this stage, switches S_1 and S_2 are simultaneously OFF. The diodes D_{in}, D_1, D_2, and D_3 are forward- biased, whereas the diodes D_o and D_{SC} are reverse-biased. The energy of magnetizing inductance (L_m) is delivered to the secondary winding of the coupled-inductor, where it is linked in parallel with the capacitors C_3 and C_4, to charge them to a voltage level depending on the conversion ratio. Output capacitor C_o continues to release energy to output load (battery). In the time duration of stage VI, the following equations can be written based on Fig. 3(e):

$$V_{L1}^{VI} = V_{PV} + V_{C_2} + V_{L_2}^{VI} - V_{C_1} \tag{8}$$

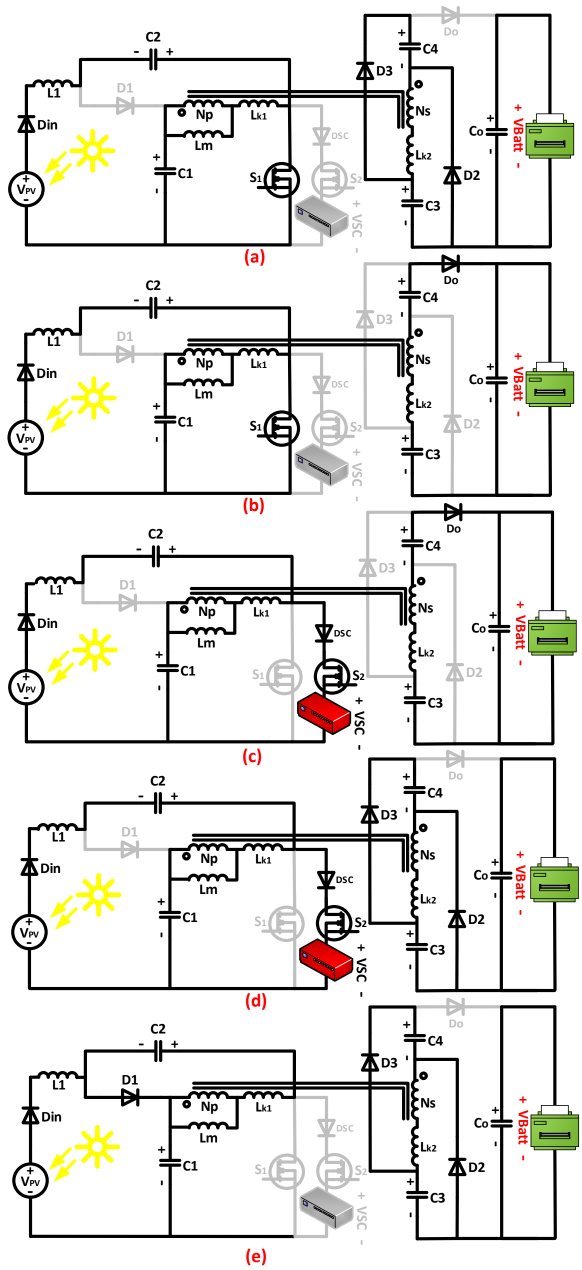

Figure 3. Topological stages of the proposed dual-output DC-DC converter; (a) $t_0 < t < t_1$, (b) $t_1 < t < t_3$, (c) $t_3 < t < t_4$, (d) $t_4 < t < t_5$, (e) $t_5 < t < t_6$

$$V_{L2}^{VI} = -V_{C_2} \tag{9}$$

Substituting (9) into (8) yields:

$$V_{L1}^{VI} = V_{PV} - V_{C_1} \tag{10}$$

Also following equations are valid.

$$V_{L_3}^{VI} = -V_{C_3} = -V_{C_4} = NV_{Lm}^{VI} \tag{11}$$

$$V_{Lm}^{VI} = -\beta V_{C_2} \tag{12}$$

Substituting (12) into (11) yields:

$$V_{C_3} = V_{C_4} = N\beta V_{C_2} \tag{13}$$

4. Steady State Analysis

The time durations I, II and IV are neglected, because they are very short and have no significant effect on steady state analysis. By applying voltage-second balance principle on the input inductor and coupled-inductor during the turn ON and OFF states of switches S_1 and S_2, the following equations can be obtained.

$$\int_0^{T_s} V_{L_2} dt = 0 \tag{14}$$

Substituting (2), (6) and (9) into (14) yields:

$$\int_0^{d_1 T_s} V_{L_2}^{III} dt + \int_0^{(d_2)T_s} V_{L_2}^{V} dt + \int_0^{(1-d_1-d_2)T_s} V_{L_2}^{VI} dt = 0 \Rightarrow$$
$$d_1 V_{C_1} + d_2(V_{C_1} - V_{SC}) + (1-d_1-d_2)(-V_{C_2}) = 0 \tag{15}$$

According to (15), it can be concluded that:

$$V_{C_1}(d_1+d_2) + V_{C_2}(d_1+d_2-1) - d_2 V_{SC} = 0 \tag{16}$$

The average voltage across V_{L1} during each switching cycle is written as:

$$\int_0^{T_s} V_{L_1} dt = 0 \tag{17}$$

Substituting (1), (5) and (10) into (17) yields:

$$\int_0^{d_1T_s} V_{L_1}^{III}\,dt + \int_0^{d_2T_s} V_{L_1}^{V}\,dt + \int_0^{(1-d_1-d_2)T_s} V_{L_1}^{VI}\,dt = 0$$
$$\Rightarrow d_1(V_{PV}+V_{C_2}) + d_2(V_{PV}-V_{SC}+V_{C_2})$$
$$+(1-d_1-d_2)(V_{PV}-V_{C_1}) = 0 \tag{18}$$

By simplifying (18), it can be concluded that:

$$V_{PV} - d_2V_{SC} + V_{C_2}(d_1+d_2) + V_{C_1}(d_1+d_2-1) = 0 \tag{19}$$

Combining (16) and (19) yields:

$$V_{PV} = V_{C_1} - V_{C_2} \tag{20}$$

Substituting (20) into (19) yields:

$$V_{C_2} = \frac{(d_1+d_2)V_{PV} - d_2V_{SC}}{1-2(d_1+d_2)} \tag{21}$$

From (4) and (20) it can be consider that:

$$V_{Batt} = N\beta(3V_{C_2} + V_{PV}) \tag{22}$$

Finally, considering (21) and (22), the voltage gain relationship for battery and SC ports will be obtained as:

$$\begin{aligned} V_{Batt} &= N\beta\left[\frac{(1+d_1+d_2)V_{PV} - 3d_2V_{SC}}{1-2(d_1+d_3)}\right] \\ V_{SC} &= \left[\frac{N\beta(1+d_1+d_2)V_{PV} - (1-2(d_1+d_3))V_{Batt}}{3d_2N\beta}\right] \end{aligned} \tag{23}$$

From (23) it can be derived that the output voltages for battery and SC are affected not only by the turn's ratio (N), but also by the duty cycles d_1 and d_2 and coupling coefficient β. Fig. 4 illustrates the available outputs voltage for battery and SC ports with several duty cycles. It can be inferred that the duty cycles have a significant impact on increasing the voltage gain of the proposed converter. Moreover, a high step up voltage gain can be realized without any extreme duty cycle or high turn's ratio.

5. Comparison Study

It is important to evaluate the performance of the proposed structure by comparison with recent on-board chargers. In order to achieve this purpose, Table 1 provides a comprehensive summary of the main circuit features of the proposed dual-output converter and some related and recent studies from the literature. In doing so, the converters in Refs. [28, 29, 34-36] have been selected. These converters are mainly used in on-board charger applications, where their main features such as voltage gain, total number of components, input current ripple and overall efficiency have been compared.

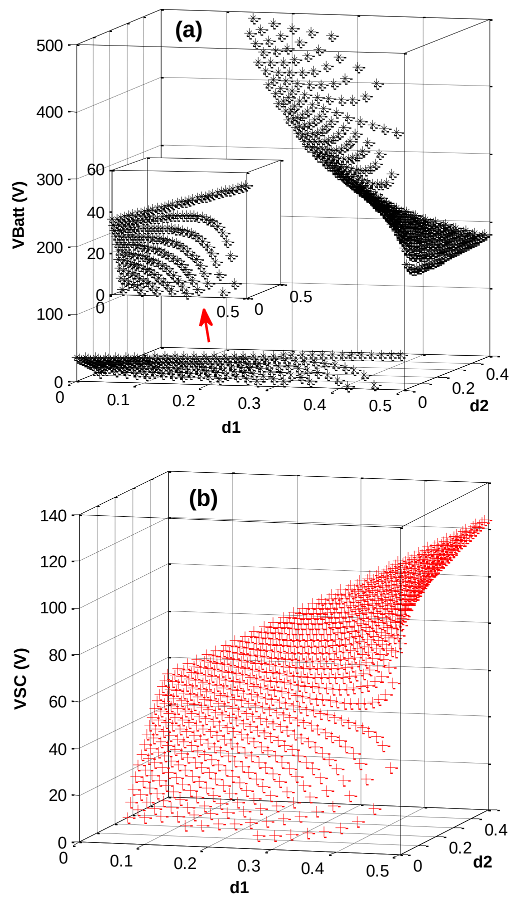

Figure 4. The available voltage for output ports: (a) battery; (b) SC

The converters in [28, 29] are without any coupled inductor and the other competitors are used coupled inductor for increasing voltage gain. Fig. 5 represents a comparison between the voltage gain ratio of the proposed charger for battery port and other aforementioned converters. From this figure it can be shown that, the voltage gain ratio of the proposed topology is higher than the others at duty cycle range only between $0<d_1<0.5$. That is because of combining the quasi Z-source network with switched capacitors that also gives it more design freedoms to supply required specifications and also leads to a wide voltage regulation with very short duty cycles. It should be noted that the turn's ratio of the coupled inductor of mentioned converters are assumed to be equal to 3. It is notable that, in the proposed topology, high voltage gain in low current stress is achieved without further increase of the turn's ratio of the coupled inductor. In terms of input current ripple, the converter in [36] and the proposed converter, which employed an additional inductor at their input port, lead them to have a low ripple continuous current at their input stage. Therefore, compared with other converters, these two topologies put lower stress on the input voltage source. In terms of the number of components, the proposed converter structure needs only two controllable power electronic switches to achieve power flows among the two loads (battery and SC) and the input source. So, the total number of switches in the proposed topology are less than the other mentioned converters. It is noteworthy that, less number of switches leads to reduced size, cost and losses of converter and also reduced number of required gate driver circuits and consequently higher efficiencies; also, the total number of capacitors are approximately equal to other relevant converters. Nevertheless, the proposed converter demonstrates a high enough efficiency against other mentioned battery chargers. The maximum efficiency of the proposed topology is about 94.66%. In overall, considering all parameters mentioned in the Table 1, it can be inferred that the proposed dual-output converter has relatively better performance than other similar devices.

Table 1: Comparison between the proposed dual-output converter and other related converters

Refs.	Types	Components (for DC-DC conversion)					Input current ripple	Ability to charge two sources at the same time	Stress on the input source	Voltage gain (G)	Eff.% (P_{out}=75 W)
		Switches	Diodes	Capacitor	Inductor	Coupled inductor/H					
[28]	Non-Isolated	9	3	1	3	0	High	No	High	$G = D/_{1-D}$	%93.34
[29]	Non-Isolated	4	4	2	2	0	High	No	High	$G = D/_{1-D}$	%94.10
[34]	Isolated	4	6	6	2	1	Moderate	No	High	$G = N_1(2\mathrm{D}+0.5\alpha),\ \alpha = N_2/_{N_1}$	%91.53
[35]	Isolated	4	8	7	2	2	Moderate	No	High	$G = N_1(2\mathrm{D}+\alpha),\ \alpha = N_2/_{N_1}$	%93.09
[36]	Isolated	6	6	5	4	1	Low	No	Low	$G = 0.5N_2/_{N_1(1-D)}$	%90.50
Proposed converter	Isolated	2	5	5	1	1	Low	Yes	Low	$Eq.\ (23)$	%94.66

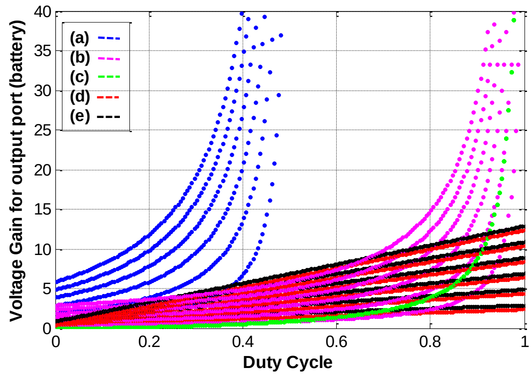

Figure 5. Voltage gain comparison: (a) proposed converter ($0<d_1<0.5$, $d_2=0$); (b) Ref. [36]; (c) Refs. [28, 29]; (d) Ref. [34]; (e) Ref. [35]

5. Simulation and Experimental Results

Computer simulations were conducted using MATLAB/Simulink environment to investigate the performance and effectiveness of the studied circuit. The simulation parameters are listed in Table 2. From the simulation results, Fig. 6 shows the MOSFETs, gate signals (V_{GS}) and the voltage of magnetizing inductor. Also, the current across magnetizing inductor along with the voltage of input inductor are shown in Fig. 7. Furthermore, the current across input inductor and the current of diode D_1 are illustrated in Fig. 8. The current of diodes D_2, D_3 and D_o are shown in Fig. 9. These results apparently are in consistent with the theoretical analysis (Fig. 2) of the proposed converter.

Due to the smaller surface of solar panels area on the roof of the SPEVs, the charging mechanism is slow; so, an alternative plug-in charging system is required to charge the batteries with a conventional AC power supply for increasing the overall utilization [3]. In doing so, the AC input must be connected to the proposed on-board charger through a suitable rectifier. In this case, from Figs. 10-13, it is proved that the proposed on-board charger has a good power quality at both input and output (for voltage and current) in term of low total harmonic distortion (THD) with well-regulated output DC voltage.

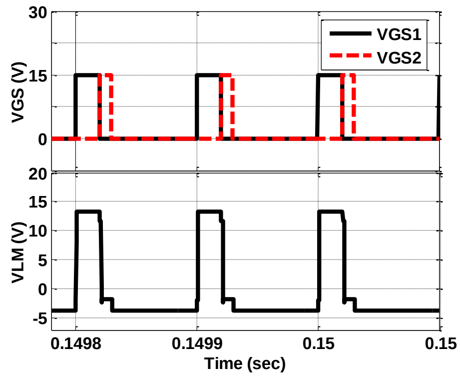

Figure 6. Simulation results: V_{GS} and V_{LM}

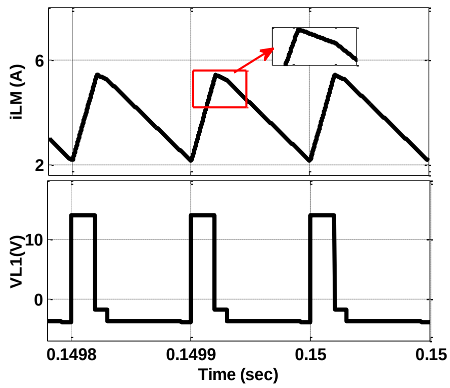

Figure 7. Simulation results: i_{LM} and V_{L1}

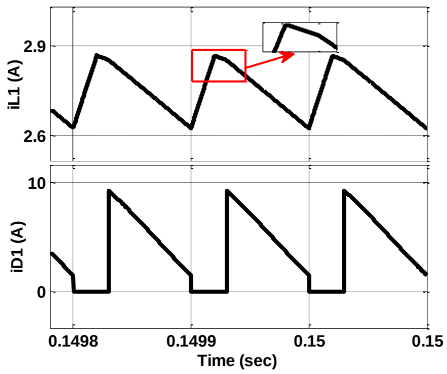

Figure 8. Simulation results: i_{L1} and i_{D1}

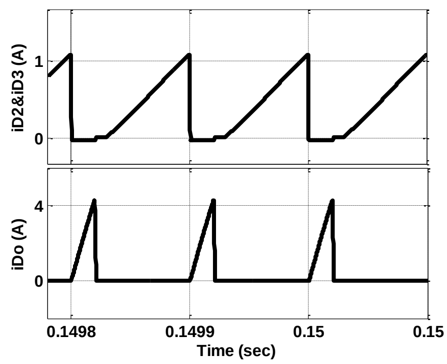

Figure 9. Simulation results: $i_{D2\&D3}$ and i_{Do}

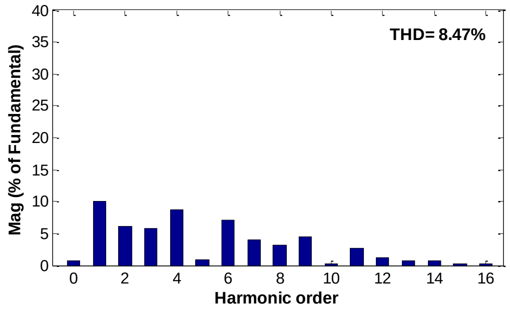

Figure 10. THD% of input AC voltage

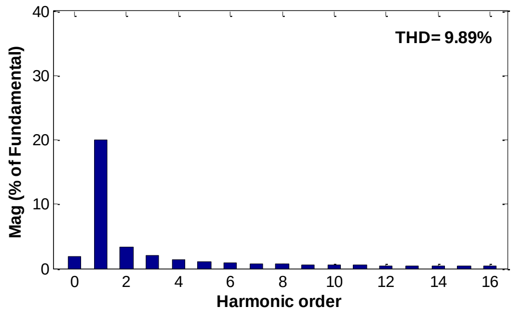

Figure 11. THD% of input AC current

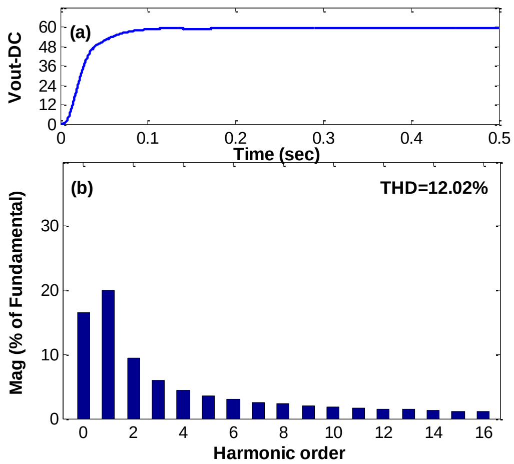

Figure 12. Harmonic Spectrum: (a) output voltage for battery port; (b) THD% of output DC voltage

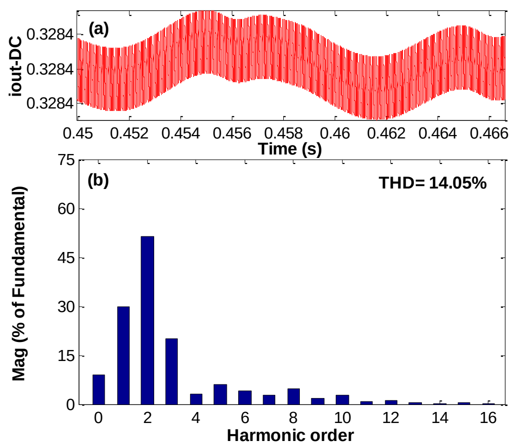

Figure 13. Harmonic Spectrum: (a) output current for battery port; (b) THD% of output DC current

In order to confirm the simulation results as well as to verify the effectiveness of the proposed dual-output converter, the prototype with 150W is realized with the specification given below.

1) PV voltage (V_{PV})=12V
2) Output voltage for battery port (V_{Batt})=60V
3) Output voltage for SC port (V_{SC})=24V
4) Switching frequency (f_{sw})= 40kHz

Fig. 14 illustrates the experimental setup of the proposed converter. A digital control board with LPC1768 ARM Cortex-M3 is employed as the controller for PWM gate pulses. Table 2 lists the circuit parameters of the prototype circuit. Due to the current limitation of the PV panels, experimental test was conducted at rate of 150 W.

One of the most important factors related to a PV system is to extract the maximum power from the PV array. Many maximum power point tracking (MPPT) algorithms and techniques investigated before. Among them perturb and observe (P&O) technique is a simple and effective method for MPPT implementation with good tracking factor [38].

Table 2: Parameters of the simulation and experimental results

Parameters	Values	
L_1	500uH - iron powder toroidal core (33 × 26 × 10)	
Coupled inductor	L_m	150uH
	L_{k1} and L_{k2}	1.5uH
	N	3(18:54)
	Core	Ferrite-EE35/42/12
C_1 and C_2	330uF (200V)	
C_3 and C_4	15uF (400V)	
C_o	680uF (450V)	
S_1 and S_2	IRFP4668 with $R_{DS}(ON)$=9.7mΩ	
D_2, D_3 and D_o	MUR4100E with maximum V_F=1.75V	
D_1, D_{in} and D_{SC}	RUR30120 with maximum V_F=2.1V	
Microcontroller	LPC1768 ARM Cortex-M3	

As indicated in Fig. 15, the MPPT is realized by sensing the current and voltage of PV and implementing P&O algorithm. Moreover, the duty cycle for all switching devices is generated through a proportional integral (PI) compensator. According to design considerations results, the turns ratio of the coupled-inducer is selected 3. To reduce the size of passive components, the switching frequency (f_{sw}) is selected 40KHZ. All diodes are schottky and ultrafast with low forward voltage drop. The power switches are selected IRFP4668 with $R_{DS}(ON)=9.7m\Omega$. As illustrated in Fig. 16, the core type of the input inductor is iron powder toroidal core (33×26×10) and the core type of coupled-inductor is Ferrite (EE35/42/12) with 0.3 mm air gap.

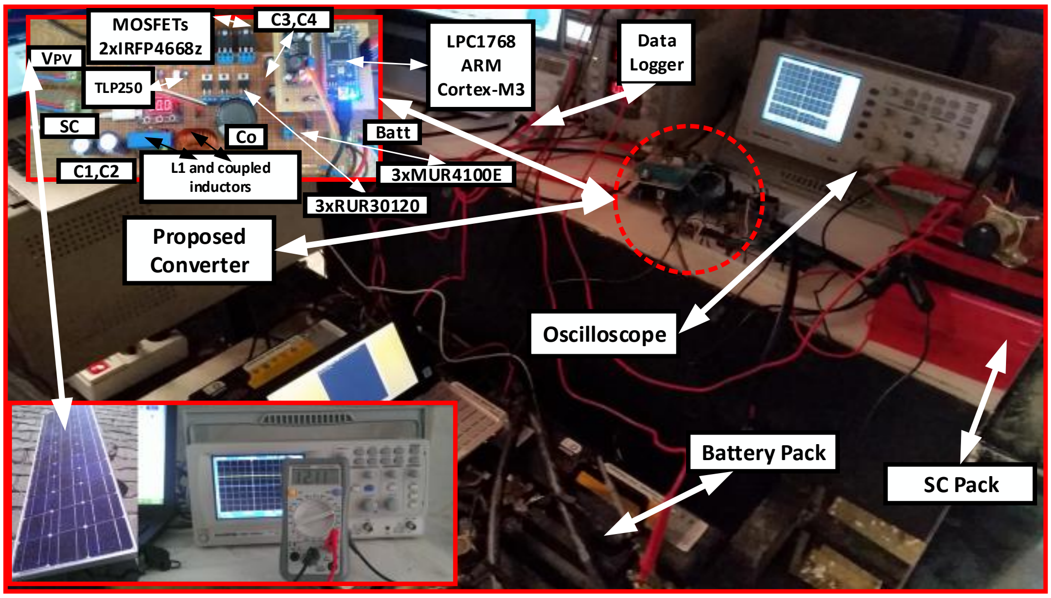

Figure 14: Test bed for hardware implementation

Fig. 17 illustrates the experimental key waveforms (voltage/current) of input and magnetizing inductors (I_{L1} and I_{LM}), diodes (i_{D1}, i_{D2}, i_{D3} and i_{Do}), capacitors (V_{C1}, V_{C2}, V_{C3} and V_{C4}), battery port (V_{Batt}), SC port (V_{SC}), and the PWM gate pulses for two MOSFETs.

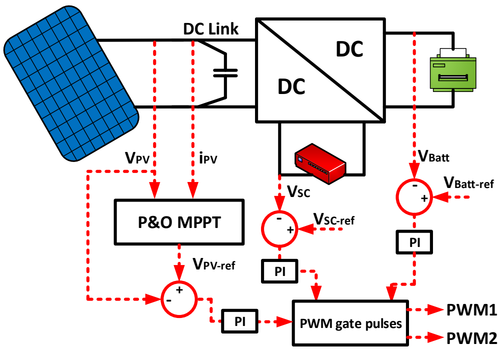

Figure 15. PV power system and PWM controller

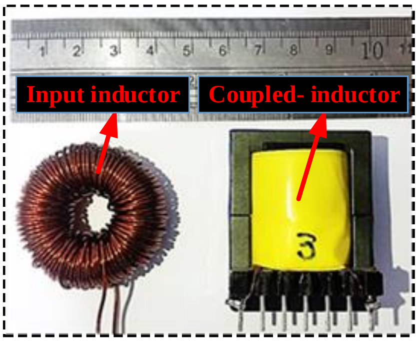

Figure 16. Input inductor and coupled-inductor of the proposed dual-output DC-DC converter

By comparing Figs. 6-9 with Fig. 17, it can be concluded that simulation results and practical results are completely consistent with each other. Also from simulation results (Figs. 7-8), the input current ripple and the magnetizing current ripple are calculated as 0.2A and 1.6A, respectively, which are in agreement with the experimental results (Fig. 17).

Apparently, the calculated values from (18-23) are in consistent with the experimental results shown in Fig. 17. The measured efficiency curves of the power stage for two output voltages, 60V (for battery port) and 24V (for SC port) are shown in the Fig. 18. The peak efficiency is measured as 94.66% for battery port.

6. Conclusions

This paper presents an on-board charger for SPEVs using a novel dual-output DC-DC converter. This topology uses impedance quasi-Z source network and also integrates both switched-capacitors and coupled-inductor techniques to achieve higher voltage gain ratio. While the proposed converter has all the benefit mentioned in the before on-board battery charger, it has fewer components and also it is capable of charging two simultaneous outputs. Theoretical analysis and design procedures have been described and explained in detail. The validity of the proposed charger was verified by simulation and experiment. Experimental results based on the designed 150W prototype circuit show 94.66% peak efficiency and high efficiency over a wide output voltage and power range. Due to its simple structure, high efficiency, and high reliability, the proposed converter is a very attractive design for SPEVs chargers.

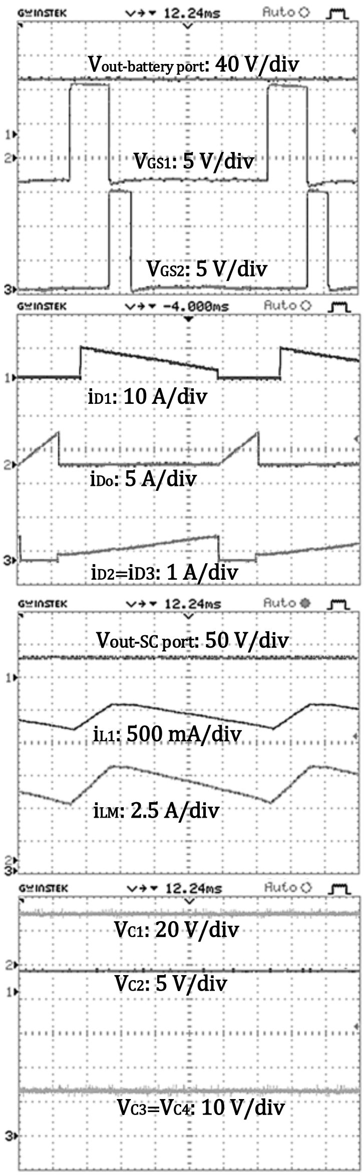

Figure 17. Experimental results

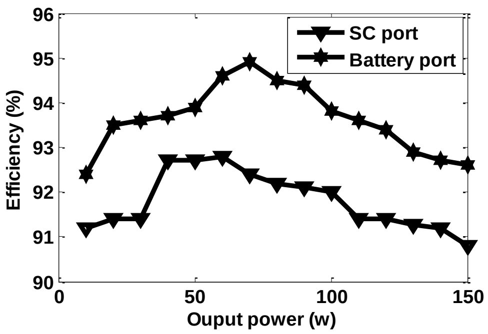

Figure 18. Measured efficiency curves

Nomenclature

Acronyms	
SPEV	Solar powered electric vehicle
HEV	Hybrid electric vehicle
PV	Photovoltaic
SC	Supercapacitor
P&O	Perturb and observe
MPPT	Maximum power point tracking
PWM	Pulse width modulation
DC	Direct current
AC	Alternating current
THD	Total harmonic distortion
MOSFET	Metal-oxide-semiconductor field-effect transistor
PI	Proportional integral
Parameters and Variables	
V_{PV}	Output voltage of the PV panels
V_{Batt}	Battery pack voltage
V_{SC}	SC pack voltage
V_{DC}	DC link voltage
V_{Ci}	Capacitors voltage
V_{Li}	Inductors voltage
V_{LM}	Magnetizing inductor voltage
i_{Li}	Inductors current
i_{LM}	Magnetizing inductor current
i_{Di}	Diodes current
D_{in}	Diode for input port
D_{SC}	Diode for supercapacitor port
D_o	Diode for output port
D_1, D_2, D_3	Diodes 1, 2 and 3
L_1	Input inductor
L_m	Magnetizing inductor
L_{K1}, L_{K2}	Leakage inductors
β	Coupling coefficient
N	Turns ratio of the coupled inductor
C_o	Output capacitor for battey port
C_1, C_2, C_3, C_4	Capacitors 1, 2, 3 and 4
S_i	Switches, i=1,2
d_i	Switches duty cycle, i=1,2
f_{sw}	Switching frequency
V_{GS}	Gate signals of the MOSFETs
$R_{DS}(ON)$	Drain-source ON resistance

References

[1] Panday, A. and Bansal, H. O. (2018). A Two-Stage Three-Phase Integrated Charger for Electric Vehicles With Dual Cascaded Control Strategy. IEEE Journal of Emerging and Selected Topics in Power Electronics, 6(2), 898–909.

[2] Aharon I. and Kuperman, A. (2011). Topological Overview of Powertrains for Battery-Powered Vehicles with Range Extenders. IEEE Transactions on Power Electronics, 26(3), 868–876.

[3] Mohammadi, F. (2018). Design, Analysis, and Electrification of a Solar-Powered Electric Vehicle. Journal of Solar Energy Research (JSER), 3(4), 293–299.

[4] Mohammadi, F. (2019). Lithium-ion Battery Market Analysis for Hybrid, Plug-in and Solar-Powered Electric Vehicles. Journal of Solar Energy Research (JSER), 4(1), 23–29.

[5] Moura, S. J., Fathy, H. K., Callaway, D. S. and Stein J. L. (2011). A stochastic optimal control approach for power management in plug-in hybrid electric vehicles. IEEE Transactions on Control Systems Technology, 19(3), 545–555.

[6] Mohammadi, F. (2018, August). Electric Vehicle Battery Market Analysis: Nickel Metal Hydride. 9th Iranian Conference on Electrical and Electronics Engineering (ICEEE).

[7] Mohammadi, F. (2018, September). Electric Vehicle Battery Market Analysis: Lead Acid. 9th Iranian Conference on Electrical and Electronics Engineering (ICEEE).

[8] Mohammadi, F. (2018, November). Electric Vehicle Battery Market Analysis: Lithium-ion. The First International Conference on Modern Approaches in Engineering Science (ICMAES).

[9] Mohammadi, F. (2018, October). Power Management Strategy in Multi-Terminal VSC-HVDC System. The 4th national Conference on Applied Research in electrical, Mechanical, Computer and IT Engineering

[10] Mohammadi, F. (2018, November). Hybridization of an Electric Vehicle Using Lithium-ion Batteries. The First International Conference on Modern Approaches in Engineering Science (ICMAES).

[11] Mohammadi, F. (2017, October). Design and Electrification of an Electric Vehicle Using Lithium-ion Batteries. 3th International Conference on Electrical Engineering.

[12] Morcos, M. M., Mersman, C. R., Sugavanam, G. D., and Dillman, N. G. (2000). Battery chargers for electric vehicles. IEEE Power Engineering Review, 20(11), 8–11.

[13] Bai, H., Zhang, Y., Semanson, C., Luo, C., and Mi, C. C. (2011). Modeling, design and optimization of a battery charger for plug-in hybrid electric vehicles. IET Electrical Systems in Transportation, 1(1), 3–10.

[14] Bai, H. and Mi, C. C. (2012). Comparison and evaluation of different DC/DC topologies for plug-in hybrid electric vehicle chargers. International Journal of Power Electronics, 4(2), 119–133.

[15] Bayat, P., Baghramian, A., Bayat, P. (2018). Implementation of hybrid electric vehicle energy management system for two input power sources. Journal of Energy Storage, 17, 423–440.

[16] Haghbin, S., Lundmark, S., Alakula, M., and Carlson O. (2011). An Isolated High-Power Integrated Charger in Electrified-Vehicle Applications. IEEE Transactions on Vehicular Technology, 60(9), 4115–4126.

[17] Jones, W. D. (2005). Take this car and plug it [plug-in hybrid vehicles. IEEE Spectrum, 42(7), 10–13.

[18] Chiang, S. J., Shieh, H., and Chen, M. (2009). Modeling and control of PV charger system with SEPIC converter. IEEE Transactions on Industrial Electronics, 56(11), 4344–4353.

[19] Lin, B. and Huang, C. (2009). Analysis and implementation of an integrated sepic-forward converter for photovoltaic-based light emitting diode lighting. IET Power Electronic, 2(6), 635–645.

[20] Melo, P. F., Gules, R., Romaneli, E. F. R. and Annunziato, R. C. (2010). A modified SEPIC converter for high-power-factor rectifier and universal input voltage applications. IEEE Transactions on Power Electronics, 25(2), 310–321.

[21] Ismail, E. H. (2009). Bridgeless SEPIC rectifier with unity power factor and reduced conduction losses," IEEE Transactions on Industrial Electronics, 56(4), 1147–1157.

[22] Chung, H. S., Ioinovici, A. and Cheung, W. (2003). Generalized structure of bidirectional switched-capacitor dc/dc converters. IEEE Transactions on Circuits and Systems, 50(6), 743–753.

[23] Law, K. K., Cheng, K. W. E. and Yeung, Y. P. B. (2005). Design and analysis of switched-capacitor-based step-up resonant converters. IEEE Transactions on Circuits and Systems, 52(5), 1998–2016.

[24] Zhang, F., Du, L., Peng, F. Z. and Qian, Z. (2008). A new design method for high-power high-efficiency switched-capacitor DC-DC converters. IEEE Transactions on Power Electronics, 23(2), 832–840.

[25] Tahavorgar, A. and Quaicoe, J. E. (2017). A dual series-resonant DC–DC converter. IEEE Transactions on Power Electronics, 32(5), 3708–3718.

[26] Zhao, Y., Li, W. and He, X. (2012). Single-phase improved active clamp coupled-inductor-based converter with extended voltage doubler

cell. IEEE Transactions on Power Electronics, 27(6), 2869–2878.

[27] Wu, T., lai, Y., Hung, J. C. and Chen, Y. (2008). Boost converter with coupled inductors and buck-boost type of active clamp. IEEE Transactions on Industrial Electronics, 55(1), 154–162.

[28] Kim, D., Kim, M., Lee, B. (2017). An Integrated Battery Charger with High Power Density and Efficiency for Electric Vehicles. IEEE Transactions on Power Electronics, 32(6), 4553 – 4565.

[29] Oh, C., Kim, D., Woo, D., Sung, W., Kim, Y., Lee, B. (2013). A High-Efficient Nonisolated Single-Stage On-Board Battery Charger for Electric Vehicles. IEEE Transactions on Power Electronics, 28(12), 5746 – 5757.

[30] Petterson, O. D. and Divan, D. M. (1991). Pseudo-resonant full bridge dc/dc converter. IEEE Transactions on Power Electronics, 6(4), 671–678.

[31] Fisher, R. A., Ngo, K. D. T. and Kuo, M. H. (1988). A 500 kHz, 250 W dc–dc converter with multiple outputs controlled by phase-shifted PWM and magnetic amplifiers. High Freq. Power Conv., 100–110.

[32] Jang, Y., Jovanovich, M. M. and Chang, Y. M. (2003). A new ZVS-PWM fullbridge converter. IEEE Transactions on Power Electronics, 18(5), 1122–1129.

[33] Boarage, M., Tiwari, S., Bhardwaj, S. and Kotaiah, S. (2008). A full-bridge DC–DC converter with zero-voltage-switching over the entire conversion ranges. IEEE Transactions on Power Electronics, 23(4), 1743–1750.

[34] Lee, I., Moon, G. (2014). Half-Bridge Integrated ZVS Full-Bridge Converter with Reduced Conduction Loss for Electric Vehicle Battery Chargers. IEEE Transactions on Industrial Electronics, 61(8), 3978 – 3988.

[35] Lee, I. (2016). Hybrid PWM-Resonant Converter for Electric Vehicle On-Board Battery Chargers. IEEE Transactions on Power Electronics, 31(5), 3639 – 3649.

[36] Lee, J. (2014). An EL Capacitorless EV On-Board Charger Using Harmonic Modulation Technique. IEEE Transactions on Industrial Electronics, 61(4), 1784 – 1787.

[37] Brito, M. A. G., Galotto, L., Sampaio, L. P., Melo, G. A. and Canesin, C. A. (2013). Evaluation of the Main MPPT Techniques for Photovoltaic Applications," IEEE Transactions on Industrial Electronics, 60(3), 1156 – 1167.